HHS Public Access

Author manuscript

J Neurosci Methods. Author manuscript; available in PMC 2020 October 01.

Published in final edited form as:

J Neurosci Methods. 2019 October 01; 326: 108362. doi:10.1016/j.jneumeth.2019.108362.

A fast machine learning approach to facilitate the detection of interictal epileptiform discharges in the scalp electroencephalogram

Elham Bagheri[a,*], **Jing Jin**[a,b,c], **Justin Dauwels**[a], **Sydney Cash**[b,c], **M. Brandon Westover**[b,c]

[a]Nanyang Technological University, School of Electrical and Electronic Engineering, Singapore 639798, Singapore

[b]Department of Neurology, Massachusetts General Hospital, Boston, MA, USA

[c]Harvard Medical School, Cambridge, MA, USA

Abstract

Background: Finding interictal epileptiform discharges (IEDs) in the EEG is a part of diagnosing epilepsy. Automated software for annotating EEGs of patients with suspected epilepsy can therefore help with reaching a diagnosis. A large amount of data is required for training and evaluating an effective IED detection system. IEDs occur infrequently in the most patients' EEG, therefore, interictal EEG recordings contain mostly background waveforms.

New Method: As the first step to detect IEDs, we propose a machine learning technique eliminating most EEG background data using an ensemble of simple fast classifiers based on several EEG features. This could save computation time for an IED detection method, allowing the remaining waveforms to be classified by more computationally intensive methods. We consider several efficient features and reject background by applying thresholds on them in consecutive steps.

Results: We applied the proposed algorithm on a dataset of 156 EEGs (93 and 63 with and without IEDs, respectively). We were able to eliminate 78% of background waveforms while retaining 97% of IEDs on our cross-validated dataset.

Comparison with Existing Methods: We applied support vector machine, k-nearest neighbours, and random forest classifiers to detect IEDs with and without initial background rejection. Results show that rejecting background by our proposed method speeds up the overall classification by a factor ranging from 1.8 to 4.7 for the considered classifiers.

Conclusions: The proposed method successfully reduces computation time of an IED detection system. Therefore, it is beneficial in speeding up IED detection especially when utilizing large EEG datasets.

GRAPHICAL ABSTRACT

[*]Corresponding author. elham001@e.ntu.edu.sg (E. Bagheri).

Disclosures

The authors have no disclosures to report.

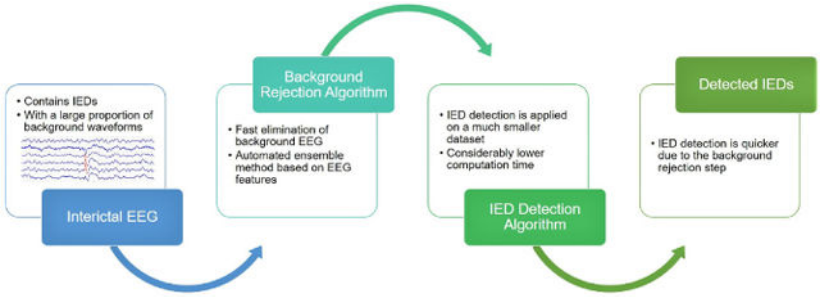

Keywords

Interictal epileptiform discharges; EEG; Machine learning; Epilepsy diagnosis; Ensemble classifier; Fast spike detection

1. Introduction

Interictal epileptiform discharges (IEDs), also called epileptiform transients (ETs) or spikes are events that occur in the scalp electroencephalogram (EEG) of patients with epilepsy between seizures. IEDs can be spikes lasting for 20–70 ms or sharp waves with pointed peaks lasting for 70–200 ms (Halford, 2009). IEDs predict recurrence of seizures following the first seizure (van Donselaar et al., 1992; Seidel et al., 2016), and they help support the diagnosis of epilepsy (Fountain and Freeman, 2006). It is important to determine if any IEDs exist in an EEG, and to find their locations (Webber and Lesser, 2017). Therefore, IED detection is instrumental for diagnosis and management of epilepsy.

In current clinical applications, the gold standard for interictal EEG interpretation is still visual inspection and manual annotation. However, a major hurdle is being tedious and subjective. Moreover, agreement among experts regarding which waveforms are epileptiform is imperfect (Halford et al., 2013, 2017; Benbadis, 2007; Castellaro et al., 2002; Wilson et al., 1996; Webber et al., 1993; Bagheri et al., 2017).

EEGs are frequently misinterpreted by neurologists without neurophysiology fellowship training, who are the majority of neurologists annotating EEGs (Benbadis, 2007). There is also considerable variability of interpretation between board-certified academic clinical neurophysiologists (Halford et al., 2013). Furthermore, experienced EEGers are in short supply (Dall et al., 2013). Misinterpreting the EEG may adversely affect patients, as it leads to misdiagnosis of epilepsy and consumption of anti-epileptic medications probably for many years; in addition, the treatment of the true underlying cause of the seizure-like events will be delayed (Benbadis, 2007). On average, patients with nonepileptic events endure seven years of anti-epileptic medication before being correctly diagnosed (Halford et al., 2013; Reuber et al., 2002). Thus, software for EEG interpretation can be useful to enhance the quality of annotations for neurologists who do not interpret EEG frequently and/or lack neurophysiology fellowship training (Halford, 2009). In addition, Bagheri et al. found that expert agreement regarding interpretation of interictal EEG is predictable when the opinion of a sufficiently large group of experts is considered (Bagheri et al., 2017). Therefore,

automated IED detection trained and validated on an adequately large EEG dataset, considering a large number of annotators, and utilizing computationally efficient algorithms offers benefits of increased speed and uniformity in EEG interpretation.

Various methods have been tried for automated IED detection including (Halford, 2009; Güler and Übeyli, 2005; Nonclercq et al., 2012; Lodder et al., 2013; Liu et al., 2013; Zhang et al., 2013; Chavakula et al., 2013; Scheuer et al., 2017). Reviews of spike analysis studies can be found in (Halford, 2009; Wilson and Emerson, 2002). However, based on the previous studies and the general opinion of experts, current systems have low sensitivity, thus neurophysiologist still must review the EEG to ensure that existing IEDs are detected (Ver Hoef et al., 2010; Halford et al., 2013). Existing systems also lack sufficient specificity, and an expert needs to look through the detections to determine the true positives (De Lucia et al., 2008; Indiradevi et al., 2008; Halford, 2009; Halford et al., 2013). Therefore, there is currently no commonly accepted IED detection software available to aid in the diagnosis of epilepsy in clinical applications.

One common problem with many methods for automated IED detection is the lack of a sufficiently large database containing various IED profiles for training and validating their performance. Consequently, they cannot be used reliably for clinical applications.

We consider a large dataset of routine scalp EEG recordings of 93 epileptic and 63 healthy subjects. We develop an ensemble of simple classifiers for rejecting most background data. The waveforms remaining from this algorithm include almost all IEDs, together with a low percentage of background waveforms that are similar to IEDs. A similar approach was taken for face detection by Viola and Jones (2004), in which they filter out over 50% of the images while preserving 99% of the faces, as a part of their face detection algorithm. The purpose of this study is to develop a fast algorithm to reliably remove non-IED (“background”) waveforms from EEG. This is particularly useful for large EEG datasets. This algorithm can serve as the initial step of an IED detection system.

In this paper, we describe the process of designing an ensemble of simple classification units for quick rejection of EEG background data, and demonstrate how employing this algorithm can speed up IED detection. By applying this algorithm on a cross-validated dataset of 156 EEGs, we eliminate 78% of background waveforms while retaining 97% of IEDs. We show that our proposed method can speed up IED detection by a factor ranging from 1.8 to 4.7 for the classifiers considered in this study.

2. Materials and methods

The purpose of this study is to develop a fast algorithm to reliably remove non-IED (“background”) waveforms from EEG. This is particularly useful with large EEG datasets. This algorithm can serve as the initial step of an IED detection system. It is a feature-based ensemble method for IED detection which detects IEDs by excluding the backgrounds. For this purpose, we need to select the best EEG features which give highest discrimination between IED and non-IED waveforms, and we employ these features to reject background

waveforms in consecutive steps. Therefore, we create a large library of features in order to pick the best ones.

2.1. EEG dataset

We consider 19-channel EEG recordings consisting of clinically-obtained scalp EEG recordings at the Massachusetts General Hospital (MGH) recorded using international 10-20 system of electrode placement. All the EEG records are re-montaged to common average reference (CAR) montage. The dataset contains 156 subjects with a total length of 4,454.2 minutes, with an average of 28.55 minutes per EEG recording. Retrospective analysis of the data was performed under an IRB-approved protocol. Among the 156 subjects, 93 are epileptic patients whose EEGs contain IEDs, and 63 are healthy subjects with IED-free EEGs. In most IED analysis studies, only EEGs from patients with epilepsy are analyzed. By contrast, here we consider the EEG from subjects without IEDs for both training and validation. The data was acquired by means of the international 10-20 system of electrode placement, and it is resampled to 128Hz. A notch filter is applied at 60 Hz for removing power line interference. Baseline drift is removed by applying a high-pass filter by cut-off frequency of 0.1 Hz. EEGs are cross-annotated by two clinical neurophysiologists from MGH using NeuroBrowser software (Jing et al., 2016). One of the experts annotated 26997 IEDs, while the other annotated 18199 IEDs. In total, there are 18,164 IEDs annotated by both experts in the dataset. We calculated the inter-rater agreement for both the annotators. The linearly weighted Gwet's agreement coefficient (AC2) (Gwet, 2001) for the experts equals 0.797. We apply 5-fold cross-validation to split the data into training and testing sets, and subjects are randomly assigned to each fold. In each round of cross-validation, we train the system on 4 folds, and test it on the 5th fold.

2.2. Data preparation and feature extraction

We propose to utilize various quick-to-compute features in consecutive steps to eliminate background waveforms from the interictal EEG. Therefore, we set out to select features which yield highest discrimination between IED and non-IED waveforms. For this purpose, we compare a library of features based on the proportion of background waveforms each of them can reject. In the remainder of this section, we explain how the features are extracted, selected, and how the system is trained, tested, and evaluated.

In this study, we analyze segments of 0.5s in duration each of them representing an IED or background. We define IEDs as waveforms that are annotated by both annotators as IED. We define backgrounds as waveforms that do not overlap with any annotated IED. We exclude the waveforms that overlap in time with any annotated IED in any channel, and we do not consider these waveforms as background. Since neurologists annotate the most prominent waveform in a particular time as IED, there may be additional IEDs on other channels at the same time instant. As the labels of such waveforms are uncertain, by excluding them we avoid training the algorithm on a potential IED regarded as background.

We compute several feature categories for each segment. Considering a large set of EEG features, allows us to select suitable discriminative ones. The categories of features, their subgroups and parameters are listed in Table 1. The choice of features is based on the

following criteria: (1) computational complexity, (2) availability of methods to compute the features, (3) literature suggesting certain features are useful for IED detection or similar applications, (4) neurologists' opinion about usefulness of certain features. We performed all data processing and statistical analysis offline in Matlab (Matlab 2014a, The Math Works Inc., Natick, MA, 2014). We now explain the features.

2.2.1. Waveform's morphological features—Morphological features computed for each 0.5 s segment include: (a) peak voltage, (b) minimum voltage, (c) peak-to-peak voltage, (d) slope, (e) duration, and (f) line length. We calculate the peak voltage as the maximum voltage of the EEG segment, the peak-to-peak voltage as the difference between maximum and minimum voltage values, the duration as the time difference between maximum and minimum voltages, and slope as peak-to-peak voltage divided by duration. We compute the line length for a signal with N points, $x(n)$ as (Esteller et al., 2001):

$$L = \Sigma_{i=1}^{N} \mid (x(k-1) - x(k)) \mid . \quad (1)$$

2.2.2. Nonlinear energy operator—NLEO is useful for detecting transient high-frequency signals, and it is commonly utilized in signal processing, image processing, and AM/FM demodulation (Maragos et al., 1993; Kaiser, 1990). NLEO accentuates high-frequency content, and due to the instantaneous nature of NLEO and having low computational burden, it is an appropriate feature to be used in IED detection (Mukhopadhyay and Ray, 1998). The studies that have utilized NLEO for IED detection include (Mukhopadhyay and Ray, 1998; Liu et al., 2013). NLEO is computed as:

$$\phi_k\{x[n]\} = x^2[n] - x[n-1]x[n+1], \quad (2)$$

where $x[n]$ denotes the signal at time n. NLEO is sensitive to high noisy peaks, especially in situations with low signal to noise ratio (SNR). Choi and Kim (2002) proposed an extension of NLEO called k-NLEO, defined as:

$$\phi_k\{x[n]\} = x^2[n] - x[n-k]x[n+k], \quad (3)$$

where k is the resolution parameter related to the peak width of the detected IED candidates. The extension k-NLEO is more sensitive to high-frequency signals and is more robust to out-of-band noise (Choi and Kim, 2002). We chose have values in the range of 1 to 40 for k. The NLEO value was first calculated for every sample point of the signal, and next we extracted segments from the EEG signals. We considered the standard deviation and maximum of the NLEO values as the features for each segment.

2.2.3. Wavelet analysis—The wavelet transform is a useful tool for characterizing many aspects of EEG signals including non-stationary transient events (Halford, 2009). It has been applied in several recent IED detection algorithms (Senhadji et al., 1995; Latka et al., 2003; Güler and Übeyli, 2005; Indiradevi et al., 2008).

For this study, we applied multiple wavelet transforms in order to generate features. We tested several wavelet basis functions, since it is unclear a priori which wavelets are best suited to detect IEDs. We considered 53 mother wavelets including symlets (sym), coiflets (coif), Daubechies (db), biorthogonal (bior), reverse biorthogonal (rbio), and discrete approximation of Meyer (dmey) wavelet basis families with different degrees (Mallat, 2008).

In the continuous wavelet transform (CWT), inner products are applied for measuring the similarity between a signal and the wavelet ψ. Specifically, the signal is compared to shifted and compressed or stretched versions of ψ:

$$\psi_{u,s}(t) = \frac{1}{\sqrt{s}}\psi\left(\frac{t-u}{s}\right), \tag{4}$$

where u and s are translation and scaling parameters, respectively. By varying the values of these parameters, the CWT coefficients $C(u, s)$ are obtained. The continuous wavelet transform $C(u, s)$ is derived from the mother wavelet $\psi_{u,s}(t)$ (Eq. (4)) by shifting and scaling the wavelet basis function as:

$$C(u,s) = \frac{1}{\sqrt{s}}\int_{-\infty}^{\infty} f(t)\psi_{u,s}(t)\mathrm{d}t\,. \tag{5}$$

The scale factor s determines compression or stretching. We tested differing values for the scale factor s in the range of 1 to 20. We computed features as the maximum absolute value and standard deviation of the coefficients on each segment, for the wavelet transform computed by each of the wavelet basis functions and various scaling factors.

We also calculated the discrete wavelet transform (DWT). In DWT the signal is decomposed into multiple scales. In Fig. 1, we illustrate the wavelet decomposition of signal $s[n]$, where Lo and Hi are high-pass and low-pass filters, respectively. Parameter d_i is the detail, while a_i represents the approximation at the ith level. These coefficients are obtained by convolving the signal by low-pass and high-pass filters, followed by a down-sampling step. Approximation coefficients of previous level are utilized to calculate the coefficients of current level. We illustrate an IED together with its wavelet coefficients at various levels for a Daubechies 3 (DB3) wavelet in Fig. 2.

We constructed 4 levels of decomposition for the discrete wavelet transform; we derived the detail and approximation coefficients for every level (Mallat, 2008). We then reconstructed these coefficients for every level, yielding an output of the same length as the input vector. We first calculated the wavelet coefficients for each channel as a whole, and then we extracted the coefficients for every 0.5s segment. This helps to avoid distortions at the boundaries of the segments and reduces the computational complexity. We calculated the features based on the resulting DWT coefficients, which include standard deviation, and maximum absolute value of the detail and approximation coefficients at every level. We calculated them for each segment for the DWT applied by each of the wavelets. At a sampling rate of 128 Hz, the filters applied in DWT for each decomposition scale include

the frequency ranges of d1 (32–64 Hz), d2 (16–32 Hz), d3 (8–16 Hz), d4 (4–8 Hz), a1 (0.5–32 Hz), a2 (0.5–16 Hz), a3 (0.5–8 Hz), and a4 (0.5–4 Hz).

2.2.4. Various frequency bands—In addition to extracting the above mentioned features for signals filtered between 0.5 and 128 Hz, we computed them on bandpass filtered signals in the standard EEG frequency bands defined as Delta (< 4 Hz), Theta (4–8 Hz), Alpha (8–12 Hz), Beta (12–32 Hz), and Gamma (> 32 Hz) (van Donselaar et al., 1992). We considered the combinations of these bands as well.

2.2.5. Spectrogram and power spectral density—We computed the spectrogram of the signal by applying the short time Fourier transform (STFT) (Mertins and Mertins, 1999) with Hamming windowing. We defined several features based on the power spectral density (PSD) values for each time segment of the signal: (a) mean of the PSD values, (b) maximum PSD, (c) frequency and time of the maximum PSD, and (d) standard deviation of PSD values.

In summary, we computed features which represent signal morphology, as well as various features to represent the frequency aspects of the signal, in the feature library. The aim is to find the most discriminant features among a large pool of automatically computed features, most of which might not be significantly discriminant.

2.3. Implementing the background rejection algorithm

Firstly, we train a cascade of thresholding steps by which we can retain most of the IEDs in the training set. Next, we apply the trained cascade on the test set. We show flowcharts of training and testing phases in Fig. 3a and b, respectively. At last, we evaluate the efficiency of the proposed algorithm by detecting IEDs by means of a number of common classification methods, with and without applying the background rejection algorithm. In the following, we explain the training and evaluation process in more detail.

2.3.1. Training—We randomly sampled background waveforms of length 0.5 s without replacement from EEG of the subjects in the training set. In this manner, we extracted 5 times more background waveforms than IEDs. For EEGs with zero or a small number of IEDs, we extracted a minimum of 2000 waveforms.

Next, we calculated the empirical cumulative density function (CDF) for each feature, for the background waveforms as well as IEDs. We select a threshold θ for each feature such that almost all IEDS are retained. Specifically, we set the fraction α of missed (undetected) IEDs to 0.001 and found the nearest point to it on the CDF and computed θ from the CDF of the IEDs accordingly. Next, we derived the ratio β of rejected background data for each feature from the backgrounds CDF. We sorted the features based on their rejection ratio β, and we selected the feature with highest value of β for the first step. After selecting the top feature, we applied its corresponding threshold θ on the whole training set. In this procedure, all waveforms having a value lower than the selected threshold θ for a given feature are rejected from the dataset. Waveforms having feature values higher than the threshold will be passed to the next stage.

We illustrate in Fig. 4 an example of the empirical CDF for the IEDs and background waveforms. The threshold θ which is selected such that 1 – α% of IEDs are retained, is shown as a vertical line. By applying this threshold, we eliminate β% of background data having feature values below θ. We apply a similar process in every step of the training phase.

We repeat the same process for the next steps in the background rejection cascade; for the remaining waveforms, we determine the feature with the highest ratio β, and remove more data according to its threshold, etc. The total background rejection rate (specificity) after the Lth stage is:

$$\beta_T = 1 - \prod_{\ell=1}^{L} (1 - \beta_\ell), \tag{6}$$

and the overall sensitivity S_L is:

$$S_L = (1 - \alpha)^L. \tag{7}$$

We add steps to the cascade until the rejection rate ceases to increase significantly or until sensitivity falls below a specific value.

Thresholding on each feature can be viewed as training a weak classifier. A weak classifier performs poorly and classifies with an accuracy slightly higher than a random classifier. Therefore, each weak classifier $h(w, f, \theta)$ is defined as:

$$h(w, f, \theta) = \begin{cases} 1, & \text{if } f(w) \geq \theta \\ 0, & \text{otherwise,} \end{cases} \tag{8}$$

where f represents a feature among all the considered features, w is a 0.5s window of EEG signals, and θ is the threshold set on the feature. Only waveforms for which $h(w, f, \theta) = 1$ are retained for the next stage. We illustrate the overall process for training in Fig. 3a.

2.3.2. Testing—After building the cascade, we assessed its performance on the test set. We show the testing process in Fig. 3b. We extracted the testing waveforms from all the EEG channels, by applying a sliding window with 50% (0.25 s) overlap. By contrast, in the training phase we randomly sampled the background waveforms. For each step, we computed the feature selected in the training phase for all the waveforms and then applied the thresholds specified in the training phase. We define the decision for each step as:

$$h(w, f_s, \theta_s) = \begin{cases} 1, & \text{if } f(w) \geq \theta \\ 0, & \text{otherwise.} \end{cases} \tag{9}$$

We updated the set of testing waveforms after every stage by keeping only the waveforms which were classified as IED, i.e., the segments for which $h(w, f_s, \theta_s) = 1$.

We computed the cascade's performance as the overall specificity and sensitivity in terms of IED detection.

2.3.3. Evaluating the algorithm's efficiency—In order to assess the proposed algorithm, we evaluated two classification procedures: (i) we trained an IED detector on the training set, without background rejection, and applied it on the testing set; (ii) we trained the detector on the remaining waveforms of the training set which were not rejected by the background rejection algorithm; we then applied it to classify the remaining waveforms from the testing set. We utilized the same cross-validation folds for the detectors as used for the background rejection phase. We illustrate both classification procedures in Fig. 5. In both scenarios, we calculated the time taken to classify the test data and the performance characteristics. Comparing the computation time and the IED detection accuracy of both methods, we can determine whether the proposed background rejection cascade speeds up the classification. We apply as classifiers (i)support vector machine (SVM) (Schölkopf et al., 2000; Boser et al., 1992; Schölkopf et al., 1995), (ii) random forest (Breiman, 2001), and (iii) K-nearest neighbors (KNN) (Cover and Hart, 1967) for detecting IEDs. We briefly explain these methods as follows (Kelleher et al., 2015):

SVMs are considered as error-based learning models. Training an SVM involves searching for the decision boundary, or separating hyperplane which leads to the maximum margin so that it best separates the levels of the target value. An SVM can easily be trained and is not too susceptible to overfitting. In addition, an SVM is highly effective for high-dimensional data. In this study, we applied SVM with Gaussian radial basis kernel.

Decision trees are very sensitive to changes in the dataset, and even a small change can result in different feature being selected to split the dataset at the root, the tree, and consequently in the subtrees. In bagging (bootstrap aggregating), which is an ensemble method, each model in the ensemble is trained on a random subset of the data generated by sampling with replacement. These random samples are known as bootstrap samples, and one model is produced from each bootstrap sample. However, when applying bagging on decision trees, each bootstrap sample uses only a randomly selected subset of the features. This sampling of the feature set is known as subspace sampling. It encourages the diversity of the trees within the ensemble and also reduces the training time for each tree. The combination of bagging, subspace sampling, and decision trees is known as a random forest (RF) model. We determine the number of decision trees by a 5-fold internal cross-validation on the training set.

KNN algorithm is a similarity-based learning method in which the Euclidean distance is measured between a signal and the training examples. In 1-nearest neighbor algorithm, there is a set of local models defined from a single instance. Considering only a single instance makes the algorithm sensitive to noise. Therefore, in order to dilute the dependency of the algorithm on individual instances, the set of K nearest neighbors to the signal are considered for classification. We optimize the value of K by 5-fold internal cross-validation on the training set.

3. Results

We applied the feature selection process illustrated in Fig. 4 for multiple steps in the training phase. In Fig. 6, we show the feature value computed for a 6-second EEG segment containing an IED, and the threshold θ applied on it as a horizontal line. In order to illustrate the process in this figure, we calculated the feature for all segments of 0.5-second using a sliding window spanning all sample points, i.e., one feature value is calculated for every segment starting at each time instance. The threshold is computed during the training process. We observe that by eliminating the EEG segments lower than the horizontal line, a significant portion of background waveforms are rejected.

We trained the cascade and applied it on the testing data. We list the sensitivity and specificity of the cascade after each individual step for both training and testing in Table 2 and Table 3, respectively. We also present the features selected and applied for the 10-step cascade in Table 4. We observe that the 10-step cascade rejects 78% of the background waveforms in the testing phase, while retaining 97% of the IEDs. Since this algorithm is developed for rejecting background waveforms and retaining almost all the IEDs, we must consider a sensitivity versus specificity trade-off. Therefore, we kept the sensitivity high but allowed the specificity to have lower values. Since in IED detection we do not need to detect all the IEDs, rather we only need to determine whether the EEG contains IEDs, the 3% missed IEDs do not significantly influence the outcome of an epilepsy diagnostic system.

In addition, the feature rankings obtained while training at each stage, are interesting in their own right for feature selection purposes. Among the considered features, discrete wavelet coefficients are the most discriminative based on the CDF, followed by morphologic features, continuous wavelet transform, nonlinear energy operator, and spectrogram features.

Moreover, the top features were among the ones computed on signals in lower frequency ranges. For the first stage, the ranking was as: 0.5–8 Hz (Delta and Theta bands), 8–12 Hz (Alpha band), 12–32 Hz (Beta band) and > 32 Hz (Gamma band).

From Table 4 we also observe that discrete wavelet transform coefficients are the main features selected among all other features for all the folds, and we only observe few morphological features in the list. This suggests that we can train the spike detection systems by relying on discrete wavelet analysis and morphological features. This can save the training time especially for even larger datasets.

We show the overall background rejection rates β_T after every step, for both training and testing sets in Fig. 7. It was expected that the rates increase after every step, and this raise becomes smaller after each step.

In Fig. 8, we show the sensitivity and specificity of the cascade as function of the number of IEDs in each EEG in the test set. We wish to investigate how the performance of the algorithm depends on the number of IEDs in the EEG records. We observe that the algorithm has low sensitivity for 5 patients. The algorithm's sensitivity is zero for four patients with 1, 1, 2, and 4 annotated IEDs, and it is 0.031 for one patient with 226 annotated IEDs. We depict all IEDs for the former, as well as four IEDs for the latter in Fig. 9, and

indicate them as P1, P2, P3, P4, and P5, respectively. The index of displayed IED for each patient is shown in parentheses.

On close inspection, the probable reasons that the cascade discards some IEDs illustrated in Fig. 9 and cannot discriminate them from background are: (1) small amplitudes of these waveforms; (2) they do not stand out very much from the background, i.e., several of them look very similar to the surrounding background waves; (3) some are probably mislabeled, i.e., would not be universally agreed to represent IEDs (such as P2, P3(1), P4(4), P5(1,2,3,4)).

The above-mentioned factors are also considered by experts when they judge whether a waveform is epileptiform. In summary, it seems understandable and reassuring that these waveforms are the kinds of examples being missed by the algorithm.

Fig. 8 also shows that specificity value varies among the subjects. For the EEGs with low specificity, the characteristics of background waveforms seem to be similar to IEDs, and therefore this algorithm fails to eliminate them. These waveforms must be classified in the following IED detection step.

Finally, we applied the IED detection methods with and without eliminating background waveforms. In Table 5, we present the overall computation time on the testing set for one minute of 19-channel EEG data. We measured the time for (a) background rejection cascade (as in Fig. 3b), (b) classifying the EEG with only SVM, KNN, or RF detector (as in Fig. 5a), (c) classifying by applying background rejection followed by an SVM, KNN, or RF (as in Fig. 5b).

We performed the analysis on a 3.4 GHz Intel Core i7 processor. In the reported time measurements, we considered the entire process including re-montaging, filtering, segmenting the data, feature computations, and applying the thresholds for background rejection, as well as applying the classifiers. The computation time for a 10-step cascade of background rejection was 0.16 seconds. Speed-up ratio in Table 5 refers to the ratio by which the computation time is reduced for the whole process. We observe that applying background rejection speeds up the IED detection for all considered classifiers.When we consider EEG recordings of different lengths, the computation time would be proportional to the computation time for 1-minute EEG presented in Table 5, i.e., The computation time for an L-minute 19-channel EEG would be $L\times$ computation time for 1-minute EEG.

We show the ROC and precision-recall curves for the two approaches in Fig. 10a and b, respectively. Considering a recall of 40% or more, the difference in the precision for IED detection with and without background rejection is insignificant. Therefore, although a large amount of EEG data is removed by background rejection, we do not compromise on the performance of IED detection.

Fig. 11 shows the total number of detections per minute for each EEG recording. The boxplots for healthy and epileptic subjects are presented as well. We observe that the detection rate is lower for IED-free subjects. In order to verify this observation, we applied a two-sample t-test on the two groups. The null hypothesis (H) is that the detection rates from

healthy and epileptic subjects come from independent random samples of normal distributions having equal means and equal or unequal unknown variances. Hence, the alternative hypothesis is that the data comes from populations with unequal means. After applying this test, the null hypothesis was rejected ($p = 9.98e^{-10}$). Therefore, there is a significant difference in the IED detection rates for epileptic and healthy EEGs, and the detection rate is higher for epileptic EEGs. This shows that our proposed method can help successfully discriminate between epileptic and healthy EEGs, which is the goal of IED detection studies.

4. Discussion

In order to assess the proposed background rejection method, we combined it with generic IED detectors, and compared its performance to those IED detectors without background rejection. We observed from Fig. 10 and Table 5 that combining background rejection algorithm with other detection methods helps to significantly reduce the computation time, while maintaining the IED detection accuracy. We also considered three common and efficient classifiers with varying computational complexity, hyperparameters, and optimization techniques. This suggests that by utilizing other classifiers, we can gain similar results.

We also noticed that there are few EEG recordings for which the algorithm fails to perform as expected. We analyzed these recordings in more detail and suggested possible reasons which can be beneficial for future studies. In summary, based on Fig. 8 and Fig. 9 subjects for which the algorithm has low sensitivity could have low amplitude spikes, or spikes that do not stand out from background. Similarly, in subjects for which the algorithm has low specificity, the background waveforms seem to have characteristics similar to IEDs that makes it hard for the algorithm to eliminate them. Both these kind of waveforms could be correctly classified in a more complex IED detection step following the background rejection.

Additionally, rejecting more proportion of background in IED-free subjects compared to epileptic subjects shows that this method as a preprocessing algorithm is suitable for filtering out normal EEGs and therefore can lead to less number of false positive detections in an IED-free EEG. This can be useful for subject-level EEG classification following IED detection.

In addition, it was shown that this algorithm can be regarded as a feature selection technique as well; and the feature ranking obtained in each stage, revealed the most discriminative features which can be employed to separate IEDs from background EEG activity. We observed from the feature ranking that discrete wavelet coefficients with certain wavelet basis functions are the leading features to discriminate between EEG background waveforms and IEDs.

Most methods applied in the literature analyzed relatively small EEG datasets, or EEG datasets with a small number of subjects. For instance, the study by Flanagan et al. (2003) explored 23,256 minutes of EEG recording; their dataset consists of only 26 subjects,

though. In this study, we considered a large dataset including 156 subjects with a total of 4,454.2 minutes of 19-channel EEG. Furthermore, our dataset contains 63 IED-free EEG recordings.

In addition, we applied 5-fold cross validation in this work, in contrast to most previous studies. Many studies failed to exploit different datasets for training and testing (Halford, 2009). Two studies (De Lucia et al., 2008; Van Hese et al., 2008) have applied cross-validation, however, they have used a small dataset of 8 patients and only 130 minutes of EEG (Van Hese et al., 2008), and 7 patients and 121 minutes of EEG (De Lucia et al., 2008) respectively.

Furthermore, we reported several common metrics, i.e., the number of false positive detections, sensitivity and specificity to quantify the performance of IED detection. It is important to report the false detection rate especially when there are numerous IEDs in the EEG.

Moreover, the number of IEDs in the EEG recordings is not considered in many studies while evaluating the performance metrics. We observe from Fig. 11 that IED detection in EEGs that have numerous IEDs is generally easier than in records with few IEDs, as expected. One study by Casson et al. (2009) suggests including the frequency of IEDs in each record while calculating the performance, since the record with numerous IEDs would skew the overall results. Therefore, in this study, we have reported the performance characteristics for individual EEG recordings based on their IED counts, as shown in Figs. 8 and 11.

The results also show that SVM performs better in IED detection compared to KNN and RF, while the performance of these algorithms in terms of false positive rate and sensitivity is not yet satisfactory. However, the goal of this study is to develop a procedure for background rejection, allowing us to reduce the computation time by removing irrelevant EEG segments. Other methods such as a classifier cascade proposed by Bagheri et al. (2018) can be applied to improve the performance of IED detection in terms of precision and false positive rate.

5. Conclusions

In order to design an efficient system for IED detection, we proposed an ensemble algorithm for fast multi-step background rejection on interictal EEG. We formed a cascade by setting thresholds on a large feature pool comprising several features such as morphological features, energy, continuous and discrete wavelet analyzes, nonlinear energy operator, and spectrogram features.

Results showed that by applying this algorithm, we are able to reject a large proportion of background waveforms and maintain most of the IEDs. Specifically, this method rejects 78% of the background waveforms while retaining 97% of the IEDs. Next, we compared two classification scenarios: firstly, we applied classifiers such as support vector machine, k nearest neighbor, and random forests to classify EEG; secondly, we applied the classifiers after rejecting the background from EEG. By comparing the performance and speed of these two methods, we observed that background rejection speeds up IED detection by eliminating

most unwanted EEG portions at an initial phase. The speedup ratio was ranging from 4.69 to 1.76. Since speed is a crucial factor for an IED detection system, we concluded that by utilizing this algorithm, we can save time while applying more complicated pattern recognition methods to further classify the IEDs in large EEG datasets.

One limitation of this method is that it does not improve the performance of IED detection. Rather, it only lowers the computation time. While this is the main goal of developing this algorithm, it is meaningful to make modifications in such a way that we can improve the sensitivity and false positive rate as well.

A potential way for this purpose is to apply other feature selection methods to find the feature ranking. So far, CDF value was utilized to select features for each step. Exploring other methods might change the feature order, and possibly improve the results. Using faster feature selection methods can also help us decrease the time needed to build the cascade.

Moreover, we can apply higher thresholds on the CDF and utilize more diverse features by increasing the cascade's length. Fo this purpose, we would require an even larger dataset to avoid overfitting. Considering more number of EEG subjects also leads to more reliable assessment of this method.

Our ultimate plan is to develop an efficient and reliable IED detector. Therefore, we need to further analyze the data that remains after this algorithm by more complicated classification algorithms, which are usually more computationally demanding. By filtering out a large proportion of background data by our proposed algorithm, we hope to maintain a reasonable computational complexity for the overall IED detection system.

Acknowledgments

Funding

EB was a PhD student in Nanyang Technological University, supported by the Singapore International Graduate Award (SINGA) scholarship funded by A*STAR. JJ was supported partially by SMART Innovation grant ING1510102-BIO.

References

Bagheri E, Dauwels J, Dean BC, Waters CG, Westover MB, Halford JJ, 2017 Interictal epileptiform discharge characteristics underlying expert interrater agreement. Clin. Neurophysiol 128, 1994–2005. [PubMed: 28837905]

Bagheri E, Jin J, Dauwels J, Cash S, Westover MB, 2018 Classifier Cascade to Aid in Detection of Epileptiform Transients in Interictal EEG. In: International Conference on Acoustics, Speech and Signal Processing (ICASSP) IEEE pp. 970–974.

Benbadis SR, 2007 Errors in EEGs and the misdiagnosis of epilepsy: importance, causes, consequences, and proposed remedies. Epilepsy Behav. 11, 257–262. [PubMed: 17719853]

Boser BE, Guyon IM, Vapnik VN, 1992 A training algorithm for optimal margin classifiers. In: Proceedings of the Fifth Annual Workshop on Computational Learning Theory ACM pp. 144–152.

Breiman L, 2001 Random forests. Mach. Learn 45, 5–32.

Casson AJ, Luna E, Rodriguez-Villegas E, 2009 Performance metrics for the accurate characterisation of interictal spike detection algorithms. J. Neurosci. Methods 177, 479–487. [PubMed: 19007811]

Castellaro C, Favaro G, Castellaro A, Casagrande A, Castellaro S, Puthenparampil D, Salimbeni CF, 2002 An artificial intelligence approach to classify and analyse EEG traces. Neurophysiologie Clinique/Clin. Neurophysiol 32, 193–214.

Chavakula V, Fernández IS, Peters JM, Popli G, Bosl W, Rakhade S, Rotenberg A, Loddenkemper T, 2013 Automated quantification of spikes. Epilepsy Behav. 26, 143–152. [PubMed: 23291250]

Choi J, Kim T, 2002 Neural action potential detector using multi-resolution teo. Electron. Lett 38, 1.

Cover T, Hart P, 1967 Nearest neighbor pattern classification. IEEE Trans. Inform. Theory 13, 21–27.

Dall TM, Storm MV, Chakrabarti R, Drogan O, Keran CM, Donofrio PD, Henderson VW, Kaminski HJ, Stevens JC, Vidic TR, 2013 Supply and demand analysis of the current and future us neurology workforce. Neurology 81, 470–478. [PubMed: 23596071]

De Lucia M, Fritschy J, Dayan P, Holder DS, 2008 A novel method for automated classification of epileptiform activity in the human electroencephalogram-based on independent component analysis. Med. Biol. Eng. Comput 46, 263–272. [PubMed: 18071771]

van Donselaar CA, Schimsheimer RJ, Geerts AT, Declerck AC, 1992 Value of the electroencephalogram in adult patients with untreated idiopathic first seizures. Archiv. Neurol 49, 231–237.

Esteller R, Echauz J, Tcheng T, Litt B, Pless B, 2001 Line length: an efficient feature for seizure onset detection. In: Engineering in Medicine and Biology Society. 2001. Proceedings of the 23rd Annual International Conference of the IEEE, IEEE pp. 1707–1710.

Flanagan D, Agarwal R, Wang Y, Gotman J, 2003 Improvement in the performance of automated spike detection using dipole source features for artefact rejection. Clin. Neurophysiol 114, 38–49. [PubMed: 12495762]

Fountain NB, Freeman JM, 2006 EEG is an essential clinical tool: pro and con. Epilepsia 47, 23–25. [PubMed: 17044821]

Güler I, Übeyli ED, 2005 Adaptive neuro-fuzzy inference system for classification of EEG signals using wavelet coefficients. J. Neurosci. Methods 148, 113–121. [PubMed: 16054702]

Gwet K, 2001 Handbook of inter-rater reliability: How to estimate the level of agreement between two or multiple raters. STATAXIS Publishing Company, Gaithersburg, MD.

Halford JJ, 2009 Computerized epileptiform transient detection in the scalp electroencephalogram: Obstacles to progress and the example of computerized {ECG} interpretation. Clin. Neurophysiol 120, 1909–1915. 10.1016/j.clinph.2009.08.007. [PubMed: 19836303]

Halford JJ, Arain A, Kalamangalam GP, LaRoche SM, Leonardo B, Basha M, Azar NJ, Kutluay E, Martz GU, Bethany WJ, et al., 2017 Characteristics of EEG interpreters associated with higher interrater agreement. J. Clin. Neurophysiol 34, 168–173. [PubMed: 27662336]

Halford JJ, Schalkoff RJ, Zhou J, Benbadis SR, Tatum WO, Turner RP, Sinha SR, Fountain NB, Arain A, Pritchard PB, et al., 2013 Standardized database development for EEG epileptiform transient detection: EEGnet scoring system and machine learning analysis. J. Neurosci. Methods 212, 308–316. [PubMed: 23174094]

Indiradevi K, Elias E, Sathidevi P, Nayak SD, Radhakrishnan K, 2008 A multi-level wavelet approach for automatic detection of epileptic spikes in the electroencephalogram. Comput. Biol. Med 38, 805–816. [PubMed: 18550047]

Jing J, Dauwels J, Rakthanmanon T, Keogh E, Cash S, Westover M, 2016 Rapid annotation of interictal epileptiform discharges via template matching under dynamic time warping. J. Neurosci. Methods 274, 179–190. [PubMed: 26944098]

Kaiser JF, 1990 On a simple algorithm to calculate the'energy'of a signal. In: in: Acoustics, Speech, and Signal Processing. 1990. ICASSP-90. 1990 International Conference on, IEEE pp. 381–384.

Kelleher JD, Mac Namee B, D'Arcy A, 2015 Fundamentals of machine learning for predictive data analytics: algorithms, worked examples, and case studies. MIT Press.

Latka M, Was Z, Kozik A, West BJ, 2003 Wavelet analysis of epileptic spikes. Phys. Rev. E 67, 052902.

Liu YC, Lin CCK, Tsai JJ, Sun YN, 2013 Model-based spike detection of epileptic EEG data. Sensors 13, 12536–12547. [PubMed: 24048343]

Lodder SS, Askamp J, van Putten MJ, 2013 Inter-ictal spike detection using a database of smart templates. Clin. Neurophysiol 124, 2328–2335. 10.1016/j.clinph.2013.05.019. [PubMed: 23791532]

Mallat S, 2008 A Wavelet Tour of Signal Processing: The Sparse Way. Academic Press.

Maragos P, Kaiser JF, Quatieri TF, 1993 On amplitude and frequency demodulation using energy operators. IEEE Trans. Signal Process 41, 1532–1550.

Mertins A, Mertins DA, 1999 Signal Analysis: Wavelets, Filter Banks, Time-Frequency Transforms and Applications. John Wiley & Sons, Inc.

Mukhopadhyay S, Ray G, 1998 A new interpretation of nonlinear energy operator and its efficacy in spike detection. IEEE Trans. Biomed. Eng 45, 180–187. [PubMed: 9473841]

Nonclercq A, Foulon M, Verheulpen D, Cock CD, Buzatu M, Mathys P, Bogaert PV, 2012 Cluster-based spike detection algorithm adapts to interpatient and intrapatient variation in spike morphology. J. Neurosci. Methods 210, 259–265. 10.1016/j.jneumeth.2012.07.015. [PubMed: 22850558]

Reuber M, Fernandez G, Bauer J, Helmstaedter C, Elger CE, 2002 Diagnostic delay in psychogenic nonepileptic seizures. Neurology 58, 493–495. [PubMed: 11839862]

Scheuer ML, Bagic A, Wilson SB, 2017 Spike detection: Inter-reader agreement and a statistical turing test on a large data set. Clin. Neurophysiol 128, 243–250. [PubMed: 27913148]

Schölkopf B, Burges C, Vapnik V, 1995 Extracting support data for a given task. Proceedings, First International Conference on Knowledge Discovery & Data Mining AAAI Press, Menlo Park, CA, pp. 252–257.

Schölkopf B, Smola AJ, Williamson RC, Bartlett PL, 2000 New support vector algorithms. Neural Comput. 12, 1207–1245. [PubMed: 10905814]

Seidel S, Pablik E, Aull-Watschinger S, Seidl B, Pataraia E, 2016 Incidental epileptiform discharges in patients of a tertiary centre. Clin. Neurophysiol 127, 102–107. [PubMed: 25802204]

Senhadji L, Dillenseger JL, Wendling F, Rocha C, Kinie A, 1995 Wavelet analysis of EEG for three-dimensional mapping of epileptic events. Ann. Biomed. Eng 23, 543–552. [PubMed: 7503457]

Van Hese P, Vanrumste B, Hallez H, Carroll GJ, Vonck K, Jones RD, Bones PJ, D'Asseler Y, Lemahieu I, 2008 Detection of focal epileptiform events in the EEG by spatio-temporal dipole clustering. Clin. Neurophysiol 119, 1756–1770. [PubMed: 18499517]

Ver Hoef L, Elgavish R, Knowlton RC, 2010 Effect of detection parameters on automated electroencephalography spike detection sensitivity and false-positive rate. J. Clin. Neurophysiol 27, 12–16. [PubMed: 20087204]

Viola P, Jones MJ, 2004 Robust real-time face detection. Int. J. Comput. Vision 57, 137–154.

Webber W, Lesser RP, 2017 Automated spike detection in EEG. Clin. Neurophysiol 128, 241–242. [PubMed: 27940048]

Webber WRS, Litt B, Lesser R, Fisher R, Bankman I, 1993 Automatic EEG spike detection: what should the computer imitate? Electroencephalogr. Clin. Neurophysiol 87, 364–373. [PubMed: 7508368]

Wilson S, Harner R, Duffy F, Tharp B, Nuwer M, Sperling M, 1996 Spike detection. i. correlation and reliability of human experts. Electroencephalogr. Clin. Neurophysiol 98, 186–198. [PubMed: 8631278]

Wilson SB, Emerson R, 2002 Spike detection: a review and comparison of algorithms. Clin. Neurophysiol 113, 1873–1881. [PubMed: 12464324]

Zhang J, Zou J, Wang M, Chen L, Wang C, Wang G, 2013 Automatic detection of interictal epileptiform discharges based on time-series sequence merging method. Neurocomputing 110, 35–43. 10.1016/j.neucom.2012.11.017.

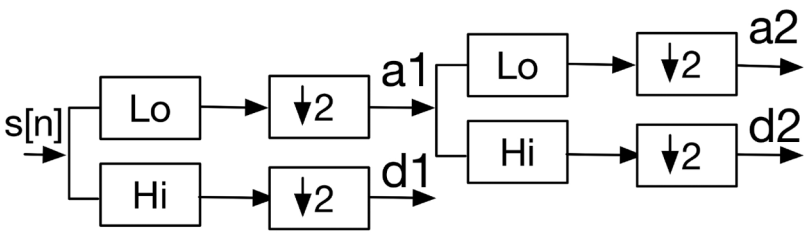

Fig. 1.
Subband decomposition for implementation of discrete wavelet transform.

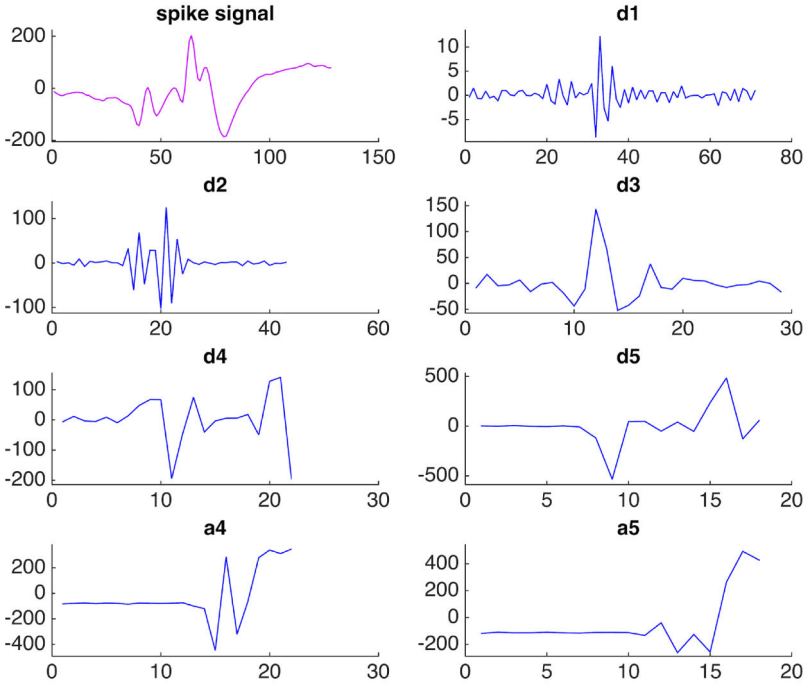

Fig. 2.
Wavelet decomposition of a sample IED.

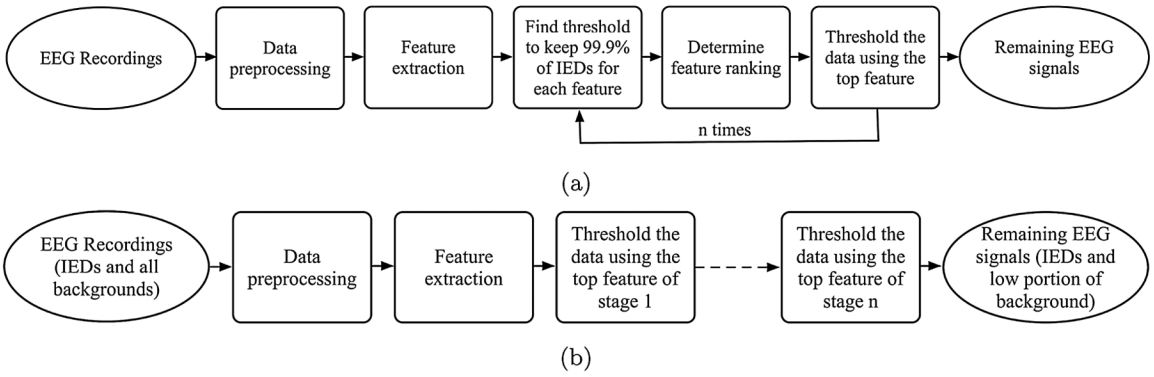

Fig. 3.
Flowcharts showing (a) training and (b) testing processes.

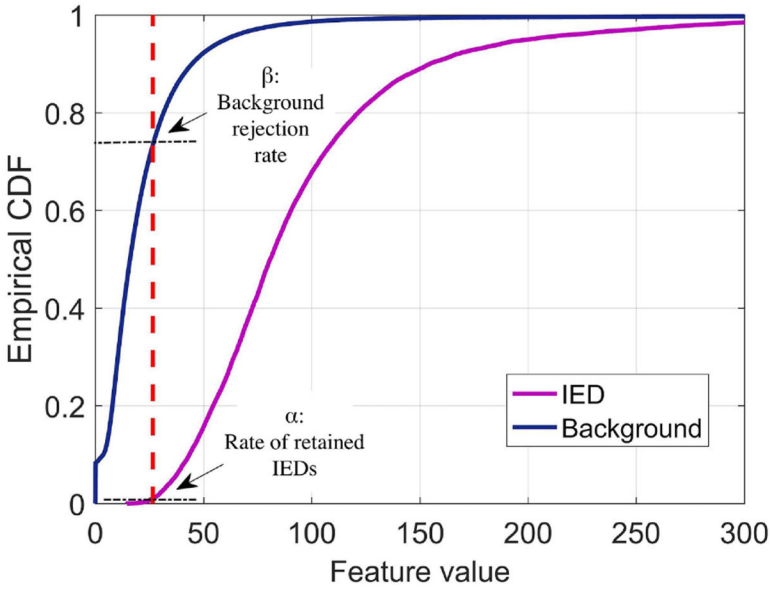

Fig. 4.

The features selection process applied in each step by computing the empirical cumulative density function.

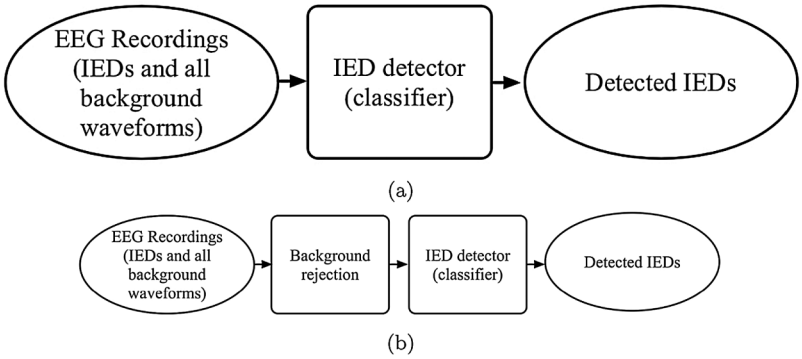

Fig. 5.

Two procedures for IED detection (a) applying a classifier; (b) applying background rejection, followed by a classifier.

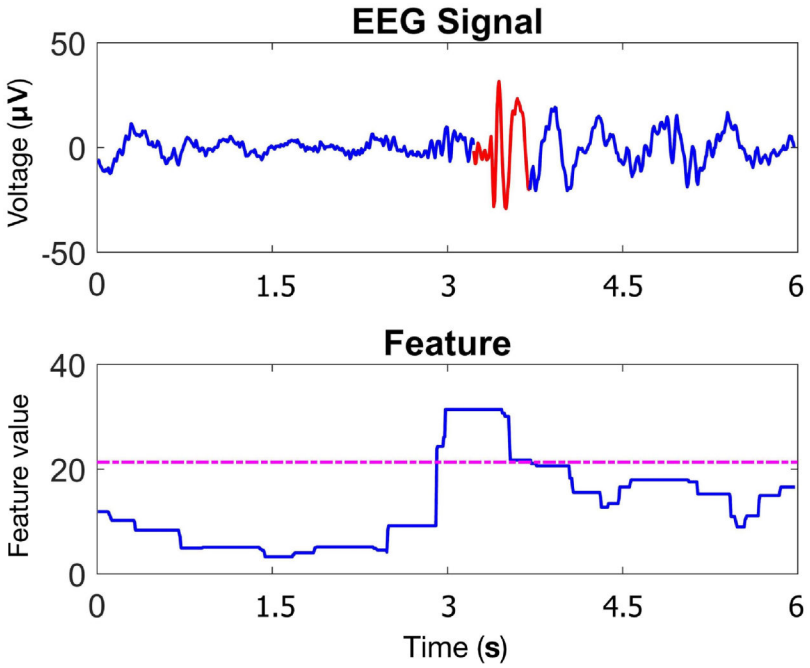

Fig. 6.

The feature DWT – rbio3.3 – max(|*a*2|), computed for a 6-second EEG segment containing an IED. The feature value is calculated for all sample points. The horizontal line shows the threshold to be applied on it, calculated during the training process.

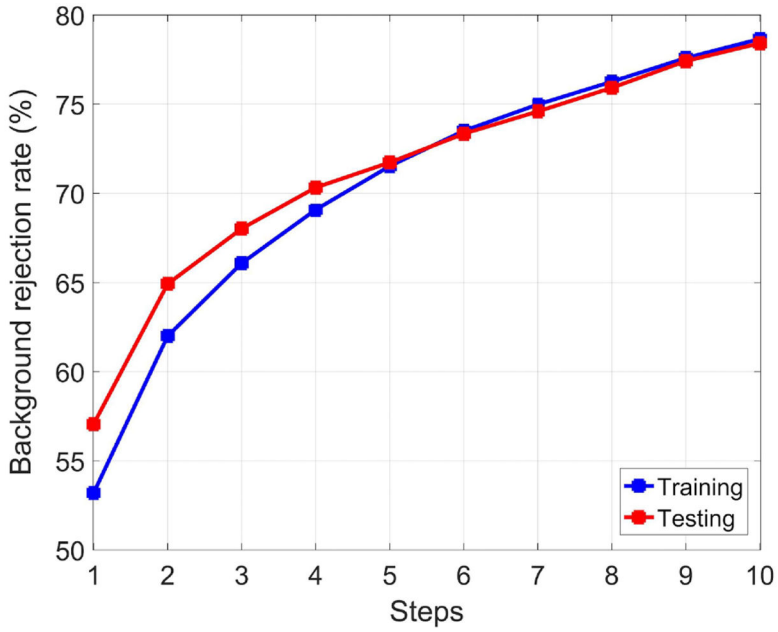

Fig. 7.
Overall percentage of rejected background after every step for training and testing sets.

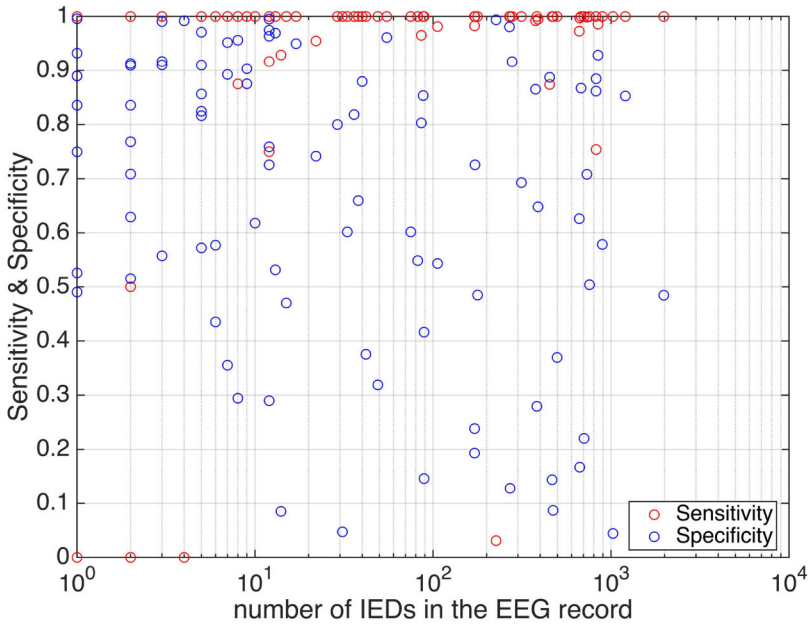

Fig. 8.
Sensitivity and specificity versus the number of IEDs in each EEG record in the test set.

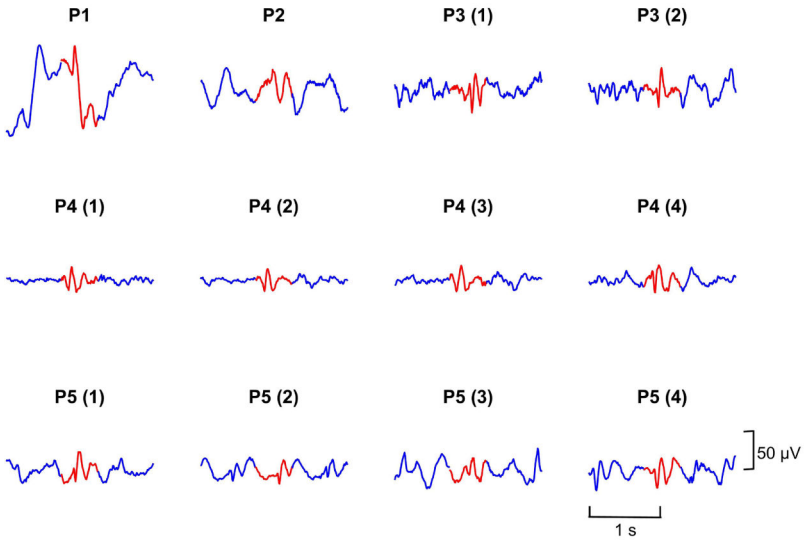

Fig. 9.

Examples of IEDs that were missed by the background rejection cascade from 5 EEGs (P1 to P5). The numbers in parentheses show the index of displayed IED for each patient.

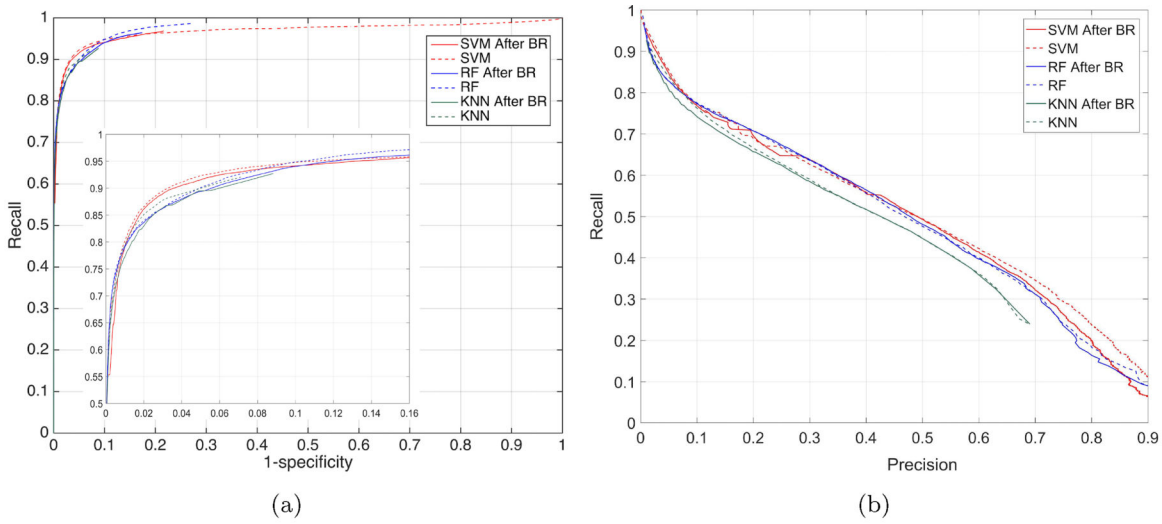

Fig. 10.

(a) ROC and (b) precision-recall curves for three classification methods with and without background rejection (BR).

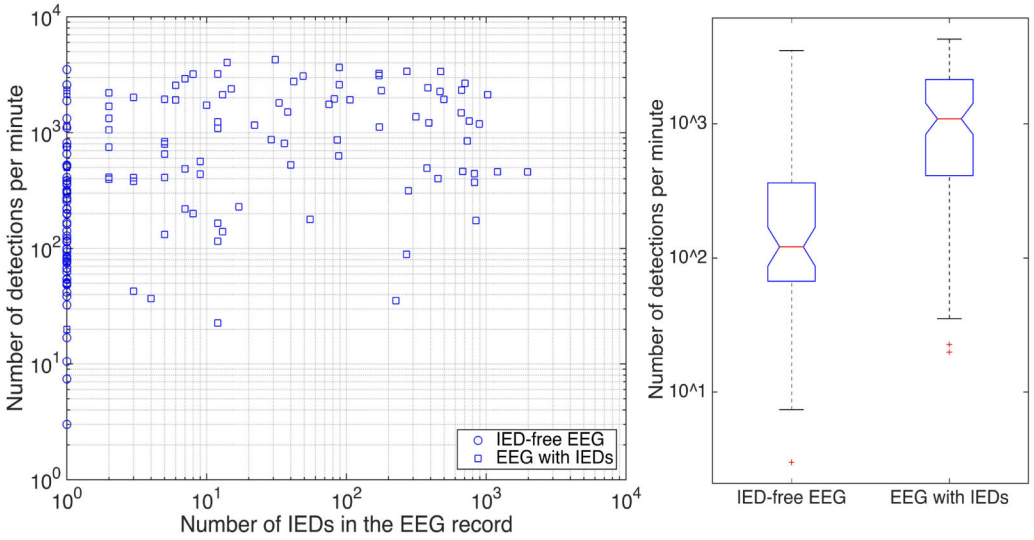

Fig. 11.

Detection rate per minute versus the number of IEDs in each EEG record for test set (left), and boxplots of detection rates for EEGs with and without IEDs (right).

Table 1

Summary of all computed feature categories, their subgroups, and their parameters.

Feature	Parameters/subgroups	
Waveform morphological features	Peak voltage, Minimum voltage,Peak-to-peak voltage, Slope,Duration, Line length	
Nonlinear energy operator	Resolution parameter k = 1 to 40	
Wavelet analysis	Continuous wavelet transform coefficients	53 wavelets, Scaling parameter s = 1 to 20
	Discrete wavelet transform coefficients	53 wavelets, 4 decomposition levels
EEG main frequency bands	Delta, Theta, Alpha, Beta, Gamma	
Spectrogram features	Mean of PSD values, Maximum PSD, Time and Frequency of maximum PSD, Standard deviation of PSD values	

J Neurosci Methods. Author manuscript; available in PMC 2020 October 01.

Table 2

Sensitivity (rate of retained IED) during training and testing for every 5 fold (F1 to F5), as well as the average over all cross-validation folds.

Steps	Training						Testing					
	F1	F2	F3	F4	F5	Mean	F1	F2	F3	F4	F5	Mean
1	0.9982	0.9981	0.9983	0.9981	0.9982	0.9982	0.9986	0.9773	1	0.9992	0.9856	0.9921
2	0.9963	0.9971	0.9965	0.9962	0.9965	0.9965	0.9957	0.966	1	0.9979	0.9831	0.9886
3	0.9945	0.9891	0.9945	0.9942	0.9952	0.9935	0.9936	0.966	0.9996	0.9979	0.9828	0.988
4	0.9933	0.9873	0.9851	0.9923	0.9933	0.9903	0.9921	0.963	0.9996	0.9979	0.9817	0.9869
5	0.9857	0.9865	0.9837	0.9837	0.9916	0.9862	0.9921	0.9621	0.9996	0.9979	0.9659	0.9835
6	0.9838	0.9851	0.9818	0.9820	0.9849	0.9835	0.9896	0.9619	0.9996	0.9975	0.9659	0.9829
7	0.9818	0.9832	0.9800	0.9802	0.9830	0.9817	0.9878	0.9611	0.9996	0.9975	0.9641	0.982
8	0.9801	0.9814	0.9784	0.9783	0.9816	0.9800	0.9796	0.9606	0.9994	0.9966	0.9634	0.9799
9	0.9785	0.9795	0.9767	0.9764	0.9800	0.9782	0.9778	0.9604	0.9994	0.9966	0.9194	0.9707
10	0.9766	0.9776	0.9749	0.9746	0.9781	0.9764	0.9739	0.9599	0.9991	0.9962	0.9176	0.9693

Table 3

Training and testing specificity (background rejection rate) for every 5 fold (F1 to F5), as well as the average over all cross-validation folds.

Steps	Training						Testing					
	F1	F2	F3	F4	F5	Mean	F1	F2	F3	F4	F5	Mean
1	0.4924	0.6369	0.5239	0.4801	0.5262	0.5319	0.5404	0.6754	0.3797	0.6068	0.6504	0.5705
2	0.5732	0.7166	0.6203	0.5957	0.5938	0.6199	0.6326	0.7594	0.4538	0.7025	0.6975	0.6492
3	0.6201	0.7441	0.6648	0.6360	0.6388	0.6608	0.6570	0.7594	0.5159	0.7432	0.7253	0.6802
4	0.6526	0.7669	0.6948	0.6652	0.6743	0.6907	0.7109	0.7804	0.5167	0.7621	0.7458	0.7032
5	0.6789	0.7830	0.7177	0.6939	0.7025	0.7152	0.7109	0.7967	0.5447	0.7621	0.7718	0.7172
6	0.7066	0.7973	0.7314	0.7124	0.7272	0.7350	0.7405	0.8071	0.5711	0.7761	0.7718	0.7333
7	0.7245	0.8077	0.7424	0.7265	0.7477	0.7497	0.7480	0.8183	0.5842	0.7888	0.7899	0.7458
8	0.7417	0.8161	0.7503	0.7420	0.7626	0.7625	0.7663	0.8278	0.5952	0.8043	0.8020	0.7591
9	0.7569	0.8238	0.7578	0.7551	0.7855	0.7758	0.7731	0.8364	0.6060	0.8137	0.8414	0.7741
10	0.7672	0.8304	0.7673	0.7658	0.8018	0.7865	0.7790	0.8433	0.6220	0.8249	0.8511	0.7841

Table 4

The features selected at every step of the cascade in the training phase.

Step	F1	F2	F3	F4	F5
1	DWT, rbio2.4, max(|*a*3|)	DWT, rbio3.3, max(|*a*2|)	DWT, rbio3.1, max(|*a*3|)	DWT, rbio4.4, max(|*a*3|)	DWT, db8, max(|*d*4|)
2	DWT, coif3, max(|*d*3|)	DWT, rbio3.1, max(|*d*1|)	DWT, db9, max(|*d*3|)	DWT, dmey, max(|*d*3|)	DWT, dmey, max(|*a*3|)
3	DWT, rbio3.3, (|*a*3|)	Peakvoltage(V_p)	DWT, db10, std(*d*4)	DWT, coif4, std(*d*4)	DWT, db9, max(|*d*3|)
4	DWT, coif5, max(|*d*3|)	DWT, bior2.4, std(*a*2)	Peakvoltage(V_p)	DWT, rbio6.8, max(|*a*3|)	DWT, dmey, max(|*d*3|)
5	Peak – to – peakvoltage(V_{pp})	DWT, rbio3.3, max(|*d*2|)	DWT, rbio1.5, max(|*a*2|)	Peak – to – peakvoltage(V_{pp})	DWT, coif5, std(*d*4)
6	DWT, sym7, max(|*d*4|)	DWT, dmey, max(|*d*3|)	DWT, sym7, std(*d*4)	DWT, rbio3.1, max(|*a*3|)	Peak – to – peakvoltage(V_{pp})
7	DWT, db6, std(*a*3)	DWT, rbio1.5, max(|*a*2|)	DWT, sym4, std(*a*2)	DWT, rbio2.4, max(|*a*2|)	DWT, db10, std(*a*3)
8	DWT, rbio2.2, max(|*d*3|)	DWT, rbio5.5, max(|*a*1|)	DWT, rbio2.8, std(*a*3)	DWT, coif4, max(|*d*3|)	DWT, rbio3.3, max(|*d*2|)
9	DWT, coif5, max(|*a*3|)	DWT, bior1.5, max(|*a*2|)	DWT, rbio1.3, std(*a*2)	DWT, coif5, max(|*a*3|)	DWT, dmey, std(*d*4)
10	DWT, db10, max(|*a*3|)	DWT, sym4, std(*a*2)	DWT, dmey, max(|*a*3|)	DWT, db10, max(|*d*4|)	DWT, db9, std(*a*3)

Table 5

Overall computation time (in seconds) on the test set for one minute of 19-channel EEG data.

Method	KNN	SVM	RF
Classifier	11.33	0.81	0.61
10-step background rejection + classifier	2.41	0.29	0.34
Speed-up ratio	4.69	2.74	1.76